Control of Voltage Source Inverter Using Multidimensional Feedback Quantization Modulator

Jwu-Sheng Hu, *Member, IEEE*, Keng-Yuan Chen, *Student Member, IEEE*, Te-Yang Shen, and Chi-Him Tang

***Abstract*—This paper describes a novel switching signal generator for three-phase voltage source inverters. Unlike conventional space-vector pulsewidth modulation (SVPWM) which achieves three-phase input voltage by a combination of the basic space vectors, the proposed scheme produces optimal switching commands to minimize the filtered measure of quantization error. Under specific selections of the filter matrix and the quantization scheme, it is shown that the proposed modulator is equivalent to SVPWM. An experimental platform is built to verify the effectiveness of the proposed scheme. It is shown that the switching number of the proposed method is reduced without sacrificing the harmonic distortion within the input frequency band under various reference signals.**

***Index Terms*—Feedback quantization, optimal control, three-phase voltage source inverter (VSI).**

I. Introduction

VARIOUS pulsewidth modulations (PWMs) have been proposed to generate the control commands of three-phase voltage source inverter (VSI) for ac variable-speed drives. To achieve a wide linear modulation range, PWMs such as third harmonic injection PWM [1], zero-sequence signal injection PWM [2], and space-vector PWM (SVPWM) considering switching state redundancy [3] are employed. For simple digital implementation, SVPWM has been developed to maintain the wide linear modulation range of line-to-line output voltage [4]–[9]. The relationship between SVPWM and carrier-based PWM is studied by shifting the efficient conducting time [5], [6], changing modulation signals [2], [10], [11], or using different zero-vector distributions [12]. Following these methods, various PWMs with different levels of performance are obtained. Notably, the unified method presented in [5] simplifies the implementation of two (or more) PWM modulators in one system for different modulation indices.

In the control of VSI, beside properties such as linear modulation range, simplicity of implementation, and total harmonic distortion (THD), an important factor is the power efficiency of the system. Since the switching loss of power MOSFETs dominates the total power loss in power converters [13], reducing the switching number without increasing the harmonic distortion is a major issue in improving power consumption and the operational lifetime of the switches [14].

However, in the PWM, the switching number of control commands is fixed once the carrier frequency is determined. For example, in the centered SVPWM [15], each switch turns on and off once per input sample; thus, the switching number is $6 \times f_c$ per second when the input is sampled at f_c Hz. Rearranging the distribution of switching commands can reduce the switching number needed in one sampling period to four without influencing the output average voltage of VSI [7], [9], [16]. Therefore, the minimum switching number of SVPWM is $4 \times f_c$ per second for a carrier frequency of f_c Hz. Reducing the carrier frequency is the only way to further reduce the switching number. Nevertheless, the size of passive components for an output low-pass filter and the THD of output currents increases as the carrier frequency is reduced [13].

Recent research works to reduce the harmonic components of the current produced involve modified SVPWM for multilevel inverters [15], [17]–[21], space-vector-based hybrid PWM [22], and optimized SVPWM [23]. In [22], the states are rearranged so that the harmonic distortion is reduced and the switching number is maintained to be comparable with that of centered SVPWM. The method in [23] employs optimal algorithm to select the active states that synthesize the reference input, to decide the usage of zero sequence and the order of the active states.

This paper focuses on the switching signal generation for three-phase two-level VSI to reduce switching number (as compared with central SVPWM) without sacrificing harmonic distortion. The multidimensional feedback quantization modulator (MDFQM) is proposed. The control of VSI with three-phase input is first formulated as a constrained optimization problem and then solved by adopting vector quantization. The relationship between MDFQM and SVPWM is also discussed. A platform is built to demonstrate the proposed modulator. Both SVPWM and MDFQM methods are implemented on a field-programmable gate array (FPGA). Experimental results tell that the proposed scheme tends to spread the noise energy over a wider band, i.e., sideband noise is reduced.

II. Theory of SVPWM

A. Power Amplifier Scheme

Fig. 1 shows the simplified structure of a three-phase VSI, where V_{a0}, V_{b0}, and V_{c0} are the output voltages of the inverter (with reference to ground). Each switch is composed of a semiconductor and a free-wheeling diode. Two switching states

Manuscript received March 29, 2010; revised July 8, 2010; accepted August 13, 2010. Date of publication September 2, 2010; date of current version June 15, 2011. This work was supported by the National Science Council of the Republic of China, Taiwan, under Contract NSC 99-2221-E-009-187.

The authors are with the Department of Electrical and Control Engineering, National Chiao Tung University, Hsinchu 300, Taiwan (e-mail: jshu@cn.nctu.edu.tw; bettery.ece94g@nctu.edu.tw; deryangshen@gmail.com; Tangch12@hotmail.com).

Digital Object Identifier 10.1109/TIE.2010.2070781

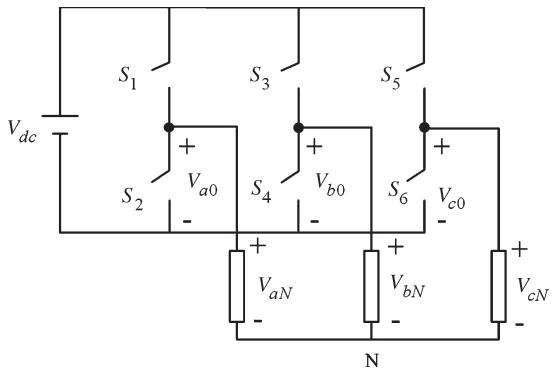

Fig. 1. Three-phase VSI topology.

exist in one bridge leg: Only the upper or the lower switch is turned on. The switching state is denoted as $+1$ (0) when the upper (lower) switch of the half bridge is turned on, such that the inverter output voltage is connected to the positive supplied voltage (ground). The switching states are represented by a vector $[a\ b\ c]^{\mathrm{T}}$, where $a, b, c \in \{0, 1\}$, indicating the state of each leg. The following equations give the relationship among line-to-line voltage $[V_{ab}\ V_{bc}\ V_{ca}]^{\mathrm{T}}$, phase voltage $[V_{aN}\ V_{bN}\ V_{cN}]^{\mathrm{T}}$, and the switching state:

$$\begin{bmatrix} V_{ab} \\ V_{bc} \\ V_{ca} \end{bmatrix} = V_{\mathrm{dc}} \begin{bmatrix} 1 & -1 & 0 \\ 0 & 1 & -1 \\ -1 & 0 & 1 \end{bmatrix} \begin{bmatrix} a \\ b \\ c \end{bmatrix} \tag{1}$$

$$\begin{bmatrix} V_{aN} \\ V_{bN} \\ V_{cN} \end{bmatrix} = V_{\mathrm{dc}} \begin{bmatrix} 2/3 & -1/3 & -1/3 \\ -1/3 & 2/3 & -1/3 \\ -1/3 & -1/3 & 2/3 \end{bmatrix} \begin{bmatrix} a \\ b \\ c \end{bmatrix}. \tag{2}$$

B. SVPWM

Assume that the three-phase input vector is sampled at a frequency f_c. The concept of SVPWM is to switch among eight switching states such that, for each sampling period $T_c(= 1/f_c)$, the average inverter output is the same as the average reference input. For simplicity, the three-phase input/output voltage vectors are transformed into $\alpha-\beta$ coordinates using the well-known transformation matrix $\mathbf{T}_{abc-\alpha\beta}$ (3). Notably, the row vectors of $\mathbf{T}_{abc-\alpha\beta}$ are the eigenvectors of the transformation matrices in (2) that correspond to the nonzero eigenvalues

$$\mathbf{T}_{abc-\alpha\beta} = \sqrt{\frac{2}{3}} \begin{bmatrix} 1 & -1/2 & -1/2 \\ 0 & \sqrt{3}/2 & -\sqrt{3}/2 \end{bmatrix}. \tag{3}$$

Fig. 2 shows the $\alpha-\beta$ components of eight line-to-line voltages. Two zero vectors $\mathbf{U}_0$ and $\mathbf{U}_7$ correspond to the switching states $[0\ 0\ 0]^{\mathrm{T}}$ and $[1\ 1\ 1]^{\mathrm{T}}$, respectively, and six nonzero vectors specify the axes of a hexagon. The angle between any two adjacent nonzero vectors is 60°. These eight vectors $\mathbf{U}_0 \sim \mathbf{U}_7$ are called basic space vectors, and each corresponds to one switching state vector.

The $\alpha-\beta$ component of the three-phase line-to-line reference vector is denoted as $\mathbf{U}_{\mathrm{ref}}$. The purpose of SVPWM is to find out durations T_i, where $i = 0, 1, \ldots, 7$, for each basic space vector

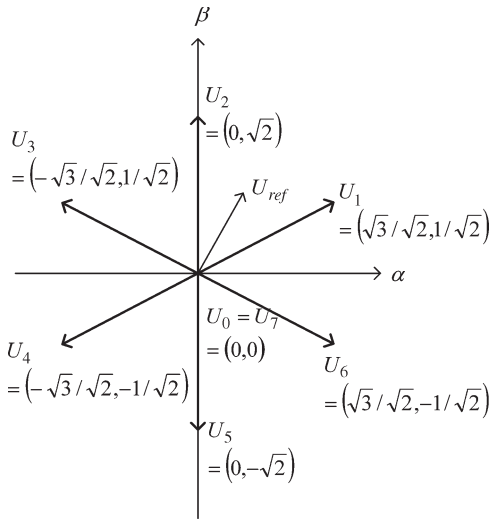

Fig. 2. Basic space vectors.

such that the average inverter output approximates the average reference input. Therefore

$$\mathbf{U}_{\mathrm{ref}}(nT_c) = \frac{1}{T_c} \sum_{i=0}^{7} T_i \mathbf{U}_i, \qquad \text{where } \sum_{i=0}^{7} T_i = T_c. \tag{4}$$

Usually, only the two nearest nonzero basic space vectors to $\mathbf{U}_{\mathrm{ref}}$ are used: $T_3 = T_4 = T_5 = T_6 = 0$ when $\mathbf{U}_{\mathrm{ref}}$ lies in the sector that is formed by $\mathbf{U}_1$ and $\mathbf{U}_2$ (Fig. 2). Equation (4) is solved easily, as shown in the following:

$$\begin{bmatrix} T_j \\ T_k \end{bmatrix} = T_c [\, \mathbf{U}_j \quad \mathbf{U}_k \,]^{-1} \mathbf{U}_{\mathrm{ref}}$$
$$T_0 + T_7 = T_c - T_j - T_k \tag{5}$$

where $j, k = 1, 2, 3, 4, 5, 6$ and $\mathbf{U}_j$ and $\mathbf{U}_k$ are the adjacent basic space vectors that form the sector that contains $\mathbf{U}_{\mathrm{ref}}$. Once the active period for each basic space vector is acquired, the switching commands in a sampling period are obtained from a lookup table.

For digital SVPWM implementation, the system clock rate is determined by the carrier frequency (reference sampling frequency) and the pulsewidth resolution. For example, the clock needed in an SVPWM system with carrier frequency f_c Hz and b-bit pulsewidth resolution is $(f_c \times 2^b)$ Hz.

III. Multidimensional Feedback Quantization

Through out this paper, the input reference $\mathbf{r}$ and output of MDFQM $\mathbf{u}$ are written as $\mathbf{u} = [u_1\ u_2\ u_3]^{\mathrm{T}}$, $\mathbf{r} = [r_1\ r_2\ r_3]^T$. Vectors $\mathbf{u}_r, \mathbf{r}_r \in R^2$ are defined as the last two elements of $\mathbf{u}$ and $\mathbf{r}$, respectively, i.e., $\mathbf{u}_r = [u_2\ u_3]^{\mathrm{T}}$, $\mathbf{r}_r = [r_2\ r_3]^{\mathrm{T}}$ and $\mathbf{u}_r = \begin{bmatrix} 0 & 1 & 0 \\ 0 & 0 & 1 \end{bmatrix} \mathbf{u}$, $\mathbf{r}_r = \begin{bmatrix} 0 & 1 & 0 \\ 0 & 0 & 1 \end{bmatrix} \mathbf{r}$. For three-phase line-to-line input vector $\mathbf{r}$ and output $\mathbf{u}$, $\mathbf{u} = \mathbf{R}_r \mathbf{u}_r$, and $\mathbf{r} = \mathbf{R}_r \mathbf{r}_r$, where $\mathbf{R}_r$ is defined as $\mathbf{R}_r = \begin{bmatrix} -1 & 1 & 0 \\ -1 & 0 & 1 \end{bmatrix}^{\mathrm{T}}$.

The set $\mathbf{S}$ which consists of the seven achievable line-to-line voltages from (1) is written as

$$\mathbf{S}=\left\{\begin{bmatrix}0\\0\\0\end{bmatrix},\begin{bmatrix}1\\0\\-1\end{bmatrix},\begin{bmatrix}0\\1\\-1\end{bmatrix},\begin{bmatrix}-1\\1\\0\end{bmatrix},\begin{bmatrix}-1\\0\\1\end{bmatrix},\begin{bmatrix}0\\-1\\1\end{bmatrix},\begin{bmatrix}1\\-1\\0\end{bmatrix}\right\}.$$

The vectors in the set $\mathbf{S}_r$, $\mathbf{w}_r \in R^2$ satisfy $\mathbf{w}_r = \begin{bmatrix}0&1&0\\0&0&1\end{bmatrix}\mathbf{w}$, where $\mathbf{w}\in\mathbf{S}$, i.e.,

$$\mathbf{S_r}=\left\{\begin{bmatrix}0\\0\end{bmatrix},\begin{bmatrix}0\\-1\end{bmatrix},\begin{bmatrix}1\\-1\end{bmatrix},\begin{bmatrix}1\\0\end{bmatrix},\begin{bmatrix}0\\1\end{bmatrix},\begin{bmatrix}-1\\1\end{bmatrix},\begin{bmatrix}-1\\0\end{bmatrix}\right\}.$$

Moreover, the vectors in the set $\mathbf{S}_{\rm pwm}$, $\mathbf{w}_{\rm pwm}\in R^2$ with n-bit resolution are written as

$$w_{\rm pwm}=l_1\mathbf{U}_i+l_2\mathbf{U}_{i\pm1}+(m-l_1-l_2)\mathbf{U}_j$$

where $m=2^n$, $i\in\{1,2,3,4,5,6\}$, $j=0$ or 7, $l_1,l_2\in\{0,1,\ldots,m\}$, and $l_1+l_2\le m$. $\mathbf{U}_i$ and $\mathbf{U}_{i\pm1}$ are the adjacent basic vectors (Fig. 2); the set $\mathbf{S}_{\rm pwm}$ represents the achievable VSI output voltage within one input period with n-bit resolution.

The MDFQM feedbacks the quantization output so that the weighted quantization error is minimized [24], [25].

A. Problem Formulation

The control of VSI can be viewed as a constrained optimization problem. The objective is to find an output vector $\mathbf{u}\in\mathbf{S}$ that approximates the three-phase input $\mathbf{r}$ over the passband of the three-input–three-output filter matrix $\mathbf{W}$. Therefore, the power of the instantaneous weighted error $\mathbf{e}(k)$ is expected to be zero. $\mathbf{e}(k)$ is the inverse z-transform of $\mathbf{E}$ defined as $\mathbf{E}=\mathbf{W}(\mathbf{R}-\mathbf{U})$, where the elements of $\mathbf{R}$ and $\mathbf{U}$ are z-transforms of the elements in $\mathbf{r}$ and $\mathbf{u}$, respectively.

The filter matrix $\mathbf{W}$ can be selected as the approximated response of VSI output load and is written in the state-space form

$$\begin{aligned}\mathbf{x}(k+1)&=\mathbf{A}\mathbf{x}(k)+\mathbf{B}\left(\mathbf{r}(k)-\mathbf{u}(k)\right)\\ \mathbf{e}(k)&=\mathbf{C}\mathbf{x}(k)+\mathbf{D}\left(\mathbf{r}(k)-\mathbf{u}(k)\right)\end{aligned}\tag{6}$$

where $\mathbf{x}\in R^p$, $\mathbf{u},\mathbf{r},\mathbf{e}\in R^3$, $\mathbf{A}\in R^{p\times p}$, $\mathbf{B}\in R^{p\times 3}$, $\mathbf{C}\in R^{3\times p}$, $\mathbf{D}\in R^{3\times 3}$, and p is the number of system states.

B. Optimal Solution

To solve the constrained output problem, first define the cost function V as the square value of $\mathbf{e}(k)$. From (6), V is written as

$$\begin{aligned}V(k)&=\mathbf{e}(k)^{\rm T}P\mathbf{e}(k)\\ &=f\left(\mathbf{x}(k),\mathbf{r}(k)\right)+\mathbf{u}(k)^{\rm T}D^{\rm T}PD\mathbf{u}(k)\\ &\quad-2\mathbf{u}(k)^{\rm T}\mathbf{D}^{\rm T}\mathbf{P}\left(\mathbf{C}\mathbf{x}(k)+\mathbf{D}\mathbf{r}(k)\right)\end{aligned}\tag{7}$$

where matrix $\mathbf{P}$ is symmetric and positive definite ($\mathbf{P}^{\rm T}=\mathbf{P}>0$), $\mathbf{Q}$ satisfies $\mathbf{Q}^{\rm T}\mathbf{Q}=\mathbf{D}^{\rm T}\mathbf{P}\mathbf{D}$, and $f(\mathbf{x}(k),r(k))$ is a term independent of $\mathbf{u}$. Intuitively, V is at its minimum when $\mathbf{u}=\mathbf{u}_u$, where $\mathbf{u}_u=\mathbf{D}^{-1}(\mathbf{C}\mathbf{x}(k)+\mathbf{D}\mathbf{r}(k))$, which is called the unconstrained optimal control force. To find the optimal $\mathbf{u}$ from the set $\mathbf{S}$ such that V is minimum, first let $\mathbf{v}=\mathbf{Q}\mathbf{u}$; then, (7) is written as

$$\begin{aligned}V(k)=f\left(\mathbf{x}(k),\mathbf{r}(k)\right)+\mathbf{v}(k)^{\rm T}\mathbf{v}(k)\\ -2\mathbf{v}(k)^{\rm T}\mathbf{Q}\mathbf{D}^{-1}\left(\mathbf{C}\mathbf{x}(k)+\mathbf{D}\mathbf{r}(k)\right).\end{aligned}\tag{8}$$

Thus, the level sets of V are spheres in R^3 that are centered at

$$\mathbf{Q}\mathbf{u}_u=\mathbf{Q}\mathbf{D}^{-1}\left(\mathbf{C}\mathbf{x}(k)+\mathbf{D}\mathbf{r}(k)\right).\tag{9}$$

Notably, the values of V for some vectors in R^3 are proportional to the distances between those vectors and $\mathbf{Q}\mathbf{u}_u$ measured in the two-norm sense. Therefore, once the nearest vector to $\mathbf{Q}\mathbf{u}_u$ in the set $\widetilde{\mathbf{S}}$ that consists of vectors $\tilde{\mathbf{w}}=\mathbf{Q}\mathbf{w}$, $\mathbf{w}\in\mathbf{S}$, is found as $\tilde{\mathbf{w}}^*$, the optimal output vector $\mathbf{u}^*$ is obtained and is of the form $\mathbf{u}^*=\mathbf{Q}^{-1}\tilde{\mathbf{w}}^*\in\mathbf{S}$.

The process of finding a nearest vector to $\mathbf{Q}\mathbf{u}_u$ in the constrained set $\widetilde{\mathbf{S}}$ is called 3-D nearest vector quantization, denoted as $q_{\widetilde{\mathbf{S}}}\{.\}$, i.e., $q_{\widetilde{\mathbf{S}}}\{\mathbf{Q}\mathbf{u}_u\}=\tilde{\mathbf{w}}^*$, and the output command $\mathbf{u}$ can be written in the form

$$\mathbf{u}=\mathbf{Q}^{-1}\tilde{\mathbf{w}}^*=\mathbf{Q}^{-1}q_{\widetilde{\mathbf{S}}}\{\mathbf{Q}\mathbf{u}_u\}.\tag{10}$$

Equation (10) indicates that the unconstrained optimal control force $\mathbf{u}_u$ is first mapped to the space that is defined by the columns of $\mathbf{Q}$, to find the constrained control force, and then transferred back to the original space by applying $\mathbf{Q}^{-1}$. A different filter matrix $\mathbf{W}$ or different cost function (different matrix $\mathbf{P}$ in (7)) will result in a different mapping matrix $\mathbf{Q}$ and a different filtered error $\mathbf{e}$ to be minimized.

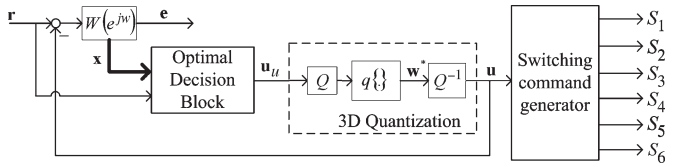

Fig. 3. Block diagram of MDFQM.

C. Multidimensional Feedback Quantization Modulator

Fig. 3 shows the block diagram of MDFQM. The switching command generator block produces control commands for switches $S_1\sim S_6$ (Fig. 1) from $\mathbf{u}$ by a lookup table. Assume that the sampling frequency of input $\mathbf{r}$ is f_c and the oversampling ratio is m. The system is operated at the frequency mf_c.

The optimal decision block computes the unconstrained optimal control force according to (9). Then, the quantization block that is composed of a space mapping module and the nearest vector quantizer computes a constrained control force that belongs to the set $\mathbf{S}$.

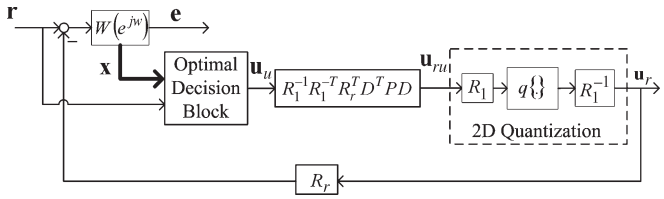

Fig. 4. Block diagram of MDFQM with reduced order.

D. Vector Quantization With Reduced Dimension

With three-phase input $\mathbf{r}$ and the three-phase VSI output voltage $\mathbf{u}$, the 3-D solution in (10) can be transformed into a 2-D expression, as described in Proposition 1.

Proposition 1: The system given by (6) and (7) with control signals $\mathbf{u}$ obtained by (9) and (10) and three-phase input $\mathbf{r}$ is equivalent to the system

$$\mathbf{x}(k+1) = \mathbf{A}\mathbf{x}(k) + \mathbf{B}\left(\mathbf{r}(k) - \mathbf{R}_r\mathbf{u}_r(k)\right)$$
$$\mathbf{e}(k) = \mathbf{C}\mathbf{x}(k) + \mathbf{D}\left(\mathbf{r}(k) - \mathbf{R}_r\mathbf{u}_r(k)\right)$$

with control signals $\mathbf{u}_r = \mathbf{R}_1^{-1} q_{\widetilde{\mathbf{S}}_r}\{\mathbf{R}_1\mathbf{u}_{ru}\}$, where $\mathbf{x} \in R^p$, $\mathbf{A} \in R^{p\times p}$, $\mathbf{B} \in R^{p\times 3}$, $\mathbf{C} \in R^{3\times p}$, and $\mathbf{D} \in R^{3\times 3}$. The matrix $\mathbf{R}_1 \in R^{2\times 2}$ satisfies

$$\mathbf{R}_r^{\mathrm{T}}\mathbf{D}^{\mathrm{T}}\mathbf{P}\mathbf{D}\mathbf{R}_r = \mathbf{R}_1^{\mathrm{T}}\mathbf{R}_1 \tag{11}$$

and $\mathbf{u}_{ru} = \mathbf{R}_1^{-1}\mathbf{R}_1^{-\mathrm{T}}\mathbf{R}_r^{\mathrm{T}}\mathbf{D}^{\mathrm{T}}\mathbf{P}(\mathbf{C}\mathbf{x}(k) + \mathbf{D}\mathbf{r}(k))$, where the image of the 2-D nearest vector quantizer denotes the vectors in the set $\tilde{\mathbf{S}}_r$, denoted as $\tilde{\mathbf{w}}_r$, satisfying $\tilde{\mathbf{w}}_r = \mathbf{R}_1\mathbf{w}_r$.

Proof: For $\mathbf{u} = \mathbf{R}_r\mathbf{u}_r$, the cost function in (7) is written as a function of the 2-D vector $\mathbf{v}_r \triangleq \mathbf{R}_1\mathbf{u}_r \in R^2$

$$\begin{aligned} V(k) &= \mathbf{e}(k)^{\mathrm{T}}\mathbf{P}\mathbf{e}(k) \\ &= f\left(\mathbf{x}(k), \mathbf{r}(k)\right) + \mathbf{v}_r(k)^{\mathrm{T}}\mathbf{v}_r(k) \\ &\quad - 2\mathbf{v}_r(k)^{\mathrm{T}}\mathbf{R}_1^{-\mathrm{T}}\mathbf{R}_r^{\mathrm{T}}\mathbf{D}^{\mathrm{T}}\mathbf{P}\left(\mathbf{C}\mathbf{x}(k) + \mathbf{D}\mathbf{r}(k)\right). \end{aligned} \tag{12}$$

The unconstrained optimal control command $\mathbf{u}_{ru}$ is defined as a 2-D vector in which the cost function (12) is minimized

$$\mathbf{v}_{ru} \triangleq \mathbf{R}_1\mathbf{u}_{ru} = \mathbf{R}_1^{-\mathrm{T}}\mathbf{R}_r^{\mathrm{T}}\mathbf{D}^{\mathrm{T}}\mathbf{P}\left(\mathbf{C}\mathbf{x}(k) + \mathbf{D}\mathbf{r}(k)\right). \tag{13}$$

The nearest vector quantization is then a 2-D quantizer with output

$$\mathbf{u}_r = \mathbf{R}_1^{-1} q_{\widetilde{\mathbf{S}}_r}\{\mathbf{R}_1\mathbf{u}_{ru}\}. \tag{14}$$

■

The reduced dimensionality of MDFQM means that, although the size of control vector $\mathbf{u}$ is three, the optimization problem involves only two degrees of freedom. Fig. 4 shows the block diagram of the reduced MDFQM, and the 2-D vector quantization can be easily implemented using an arithmetic expression, as discussed in [24] and [25].

E. Relationship Between SVPWM and MDFQM

In SVPWM, input $\mathbf{r}$ and output $\mathbf{u}$ are mapped on the $\alpha-\beta$ plane to simplify the calculation. Control commands are then generated in the sense that the average VSI output voltage approximates the average reference input. In the proposed MDFQM with reduced dimensions, the unconstrained optimal control force $\mathbf{u}_{ru}$ is initially mapped to a space that is defined by the columns of matrix $\mathbf{R}_1$ [see (12)–(14)], and then, the system produces the control $\mathbf{u}$ via the nearest vector quantizer.

This section demonstrates that there exist $\mathbf{W}$ and $\mathbf{P}$ such that the mapping matrix $\mathbf{R}_1$ mapped the vector $\mathbf{u}_{ru}$ onto the $\alpha-\beta$ plane with exactly the same coordinates as SVPWM. Therefore, under a specific image of the quantizer, SVPWM is a special case of the MDFQM.

Proposition 2: The MDFQM system described in Proposition 1 is exactly an n-bit resolution SVPWM when the following conditions are satisfied.

1) $\mathbf{W}$ is a diagonal filter matrix with a pure integrator on its diagonal.
2) The oversampling ratio is $m = 2^n$, and zero-order hold is used as an up sampler for input reference $\mathbf{r}$.
3) The cost function is defined as
$$V(k) = \mathbf{e}(mk+m)^{\mathrm{T}}\mathbf{e}(mk+m).$$
4) The image of the nearest vector quantizer $q_{\widetilde{\mathbf{S}}_{\mathrm{pwm}}}\{.\}$ are vectors in the set $\widetilde{\mathbf{S}}_{\mathrm{pwm}}$, denoted as $\widetilde{\mathbf{w}}_{\mathrm{pwm}} \in R^{2\times 1}$, satisfying $\widetilde{\mathbf{w}}_{\mathrm{pwm}} = \mathbf{R}_2\mathbf{w}_{\mathrm{pwm}}$, where $\mathbf{R}_2^{\mathrm{T}}\mathbf{R}_2 = \mathbf{R}_r^{\mathrm{T}}\mathbf{R}_r$.

Proof: From assumption 1), $\mathbf{W}$ is written as

$$\mathbf{W} = \begin{bmatrix} w(z) & 0 & 0 \\ 0 & w(z) & 0 \\ 0 & 0 & w(z) \end{bmatrix}, \qquad \text{where } w(z) = \frac{z}{z-1}.$$

The state-space matrices of the system are

$$\mathbf{A} = \mathbf{B} = \mathbf{C} = \mathbf{D} = \begin{bmatrix} 1 & 0 & 0 \\ 0 & 1 & 0 \\ 0 & 0 & 1 \end{bmatrix}.$$

From 1) and (6)

$$\begin{aligned} \mathbf{e}(mk+m) &= \mathbf{x}(mk) + \sum_{i=mk+1}^{mk+m}\mathbf{r}(i) - \sum_{i=mk+1}^{mk+m}\mathbf{u}(i) \\ &= \mathbf{x}(mk) + \sum_{i=mk+1}^{mk+m}\mathbf{r}(i) - \mathbf{R}_r\sum_{i=mk+1}^{mk+m}\mathbf{u}_r(i). \end{aligned}$$

Therefore, the cost function is a function with variables $\mathbf{u}_r(i)$, $i = mk+1, mk+2, \cdots mk+m$. From 2) and the definition of $\mathbf{u}_{ar}$ as the sum of the VSI output voltages within one input period [$\mathbf{u}_{ar} = (\sum_{i=mk+1}^{mk+m}\mathbf{u}_r(i))$], the cost function is written in the form

$$\begin{aligned} V(k) &= \mathbf{e}(mk+m)^{\mathrm{T}}\mathbf{e}(mk+m) \\ &= f(\mathbf{x}, \mathbf{r}) + \mathbf{u}_{ar}^{\mathrm{T}}\mathbf{R}_r^{\mathrm{T}}\mathbf{R}_r\mathbf{u}_{ar} \\ &\quad + \mathbf{u}_{ar}^{\mathrm{T}}\mathbf{R}_r^{\mathrm{T}}\left(\mathbf{x}(mk) + m\mathbf{r}(mk+1)\right). \end{aligned} \tag{15}$$

Finding the optimal sequence $\mathbf{u}(i)$, $i = mk+1, mk+2, \cdots mk+m$ equates to finding the optimal achievable VSI

output voltage $\mathbf{u}_{ar}$. Once $\mathbf{u}_{ar}$ is known, the duty cycle for each basic vector is obtained, and the switching pattern within a single input period can be produced by the methods described with reference to the SVPWM. Equation (15) yields $\mathbf{u}_{ar}$

$$\mathbf{u}_{ar} = \mathbf{R}_2^{-1} q_{\widetilde{\mathbf{S}}_{\mathrm{pwm}}} \left\{ \mathbf{R}_2^{-\mathrm{T}} \mathbf{R}_r^{\mathrm{T}} \left(\mathbf{x}(mk) + m\mathbf{r}(mk+1) \right) \right\} \tag{16}$$

where $\mathbf{R}_2^{\mathrm{T}}\mathbf{R}_2 = \mathbf{R}_r^{\mathrm{T}}\mathbf{R}_r = \begin{bmatrix} 2 & 1 \\ 1 & 2 \end{bmatrix}$. Consequently, one can choose $\mathbf{R}_2$ as $\mathbf{R}_2 = \begin{bmatrix} -\sqrt{3}/\sqrt{2} & -\sqrt{3}/\sqrt{2} \\ \sqrt{3}/\sqrt{6} & -\sqrt{3}/\sqrt{6} \end{bmatrix}$. The input to $q_{\widetilde{\mathbf{S}}_{\mathrm{pwm}}}\{.\}$ is written as

$$\begin{aligned} &\mathbf{R}_2^{-\mathrm{T}} \mathbf{R}_r^{\mathrm{T}} \left(\mathbf{x}(mk) + m\mathbf{r}(mk+1) \right) \\ &\quad = \mathbf{R}_2^{-\mathrm{T}} \begin{bmatrix} -1 & 1 & 0 \\ -1 & 0 & 1 \end{bmatrix} \left(\mathbf{x}(mk) + m\mathbf{r}(mk+1) \right) \\ &\quad = \sqrt{\frac{2}{3}} \begin{bmatrix} 1 & -1/2 & -1/2 \\ 0 & \sqrt{3}/2 & -\sqrt{3}/2 \end{bmatrix} \left(\mathbf{x}(mk) + m\mathbf{r}(mk+1) \right) \\ &\quad = \mathbf{T}_{abc-\alpha\beta} \left(\mathbf{x}(mk) + m\mathbf{r}(mk+1) \right). \end{aligned} \tag{17}$$

Equations (16) and (17) reveal that the system first maps the 3-D vector $(\mathbf{x}(mk) + m\mathbf{r}(mk+1))$ to the $\alpha-\beta$ plane and then performs the 2-D nearest vector quantization $q_{\widetilde{\mathbf{S}}_{pwm}}\{.\}$, whose image is exactly the same as the linear combination of any two adjacent basic space vectors within one input sampling period. Therefore, it is exactly the same as the matching equation indicated in (4) if $\mathbf{x}(mk) = 0$. Because $\mathbf{x}(mk)$ is the cumulated error under condition 1), it can be written as [from (6)]

$$\mathbf{x}(mk) = \mathbf{x}\left(m(k-1)\right) + \sum_{i=mk+1}^{mk+m} \mathbf{r}(i) - \sum_{i=mk+1}^{mk+m} \mathbf{u}(i). \tag{18}$$

From 2), $\mathbf{r}(i)$ is a constant vector during $i = mk+1 \sim mk+m$. One can rewrite (18) as

$$\mathbf{x}(mk) = \mathbf{x}\left(m(k-1)\right) + m\mathbf{r}(mk+1) - \sum_{i=mk+1}^{mk+m} \mathbf{u}(i). \tag{19}$$

Now, considering the case $k = 1$ with zero initial value $(x(0) = 0)$, (19) becomes

$$\begin{aligned} \mathbf{x}(m) &= \mathbf{x}(0) + m\mathbf{r}(m+1) - \sum_{i=m+1}^{m+m} \mathbf{u}(i) \\ &= m\mathbf{r}(m+1) - \sum_{i=m+1}^{2m} \mathbf{u}(i). \end{aligned} \tag{20}$$

Because $\sum_{i=m+1}^{2m} \mathbf{u}(i)$ is selected to be equal to $m\mathbf{r}(m+1)$, we obtain $\mathbf{x}(m) = 0$. Following the procedure, it is easy to find that $\mathbf{x}(mk) = 0\ \forall k$, where k is an arbitrary positive integer. As a consequence, the MDFQM with conditions 1)–4) is exactly the SVPWM. ■

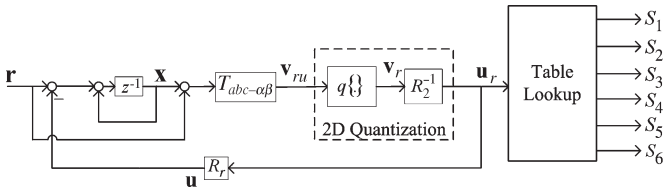

Fig. 5. Block diagram of MDFQM for implementation.

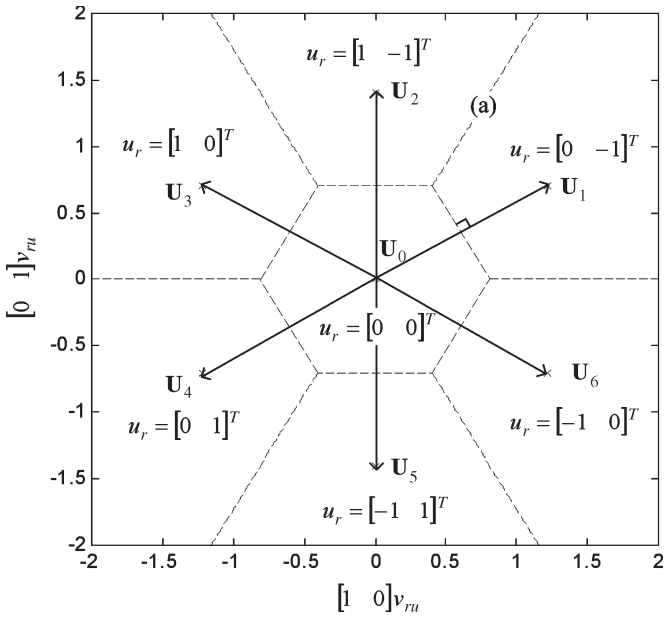

Fig. 6. Input and output relation of 2-D quantization block.

F. Implementation of the Proposed Modulator

As an illustrated example, Fig. 5 shows the block diagram of the software implementation of the system in Proposition 2. Only multipliers and adders are needed to compute the signal $\mathbf{v}_{ru}$. For implementing the 2-D quantization block, consider the case $n = 0$: $m = 1$, and the image of $q_{\widetilde{\mathbf{S}}_{\mathrm{pwm}}}\{.\}$ is exactly the seven basic vectors ($\mathbf{U}_i$, $i = 0 \sim 6$ in Fig. 2). Based on the concept of the nearest vector quantization $q_{\widetilde{\mathbf{S}}_{pwm}}\{.\}$, we have to choose among $\mathbf{U}_i$'s such that the distance between the input and output of $q_{\widetilde{\mathbf{S}}_{\mathrm{pwm}}}\{.\}$ ($\mathbf{v}_{ru}$ and $\mathbf{v}_r$ in Fig. 5) is minimized. It is straightforward to partition the $\alpha-\beta$ plane into seven regions (Fig. 6), where partition lines (the dashed lines in Fig. 6) are the perpendicular bisectors of adjacent $\mathbf{U}_i$'s. For example, line (a) is the perpendicular bisector of the line from $\mathbf{U}_1$ to $\mathbf{U}_2$. According to $\mathbf{U}_1 = (\sqrt{3/2}, \sqrt{1/2})$ and $\mathbf{U}_2 = (0, \sqrt{2})$, the equation of line (a) is easily obtained as $y = \sqrt{3}x$, where the input vector of 2-D quantization is written as $\mathbf{v}_{ru} = [x\ y]^{\mathrm{T}}$. Therefore, the partition in Fig. 6 is the input/output relation of $q_{\widetilde{\mathbf{S}}_{\mathrm{pwm}}}\{.\}$. To obtain $\mathbf{u}_r$ (see Fig. 5), $\mathbf{v}_r$ is multiplied by $\mathbf{R}_2^{-1}$. For instance, when output of $q_{\widetilde{\mathbf{S}}_{\mathrm{pwm}}}\{.\}$, $\mathbf{v}_r$, is $\mathbf{U}_2 = (0, \sqrt{2})$, then

$$\mathbf{u}_r = \mathbf{R}_2^{-1}\mathbf{U}_2 = \begin{bmatrix} -1/\sqrt{6} & 1/\sqrt{2} \\ -1/\sqrt{6} & -1/\sqrt{2} \end{bmatrix} \begin{bmatrix} 0 \\ \sqrt{2} \end{bmatrix} = \begin{bmatrix} 1 \\ -1 \end{bmatrix}.$$

The corresponding $\mathbf{u}_r$ for each partition is also shown in Fig. 6.

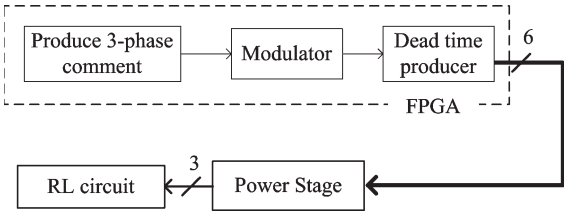

Fig. 7. Block diagram of the implementation platform.

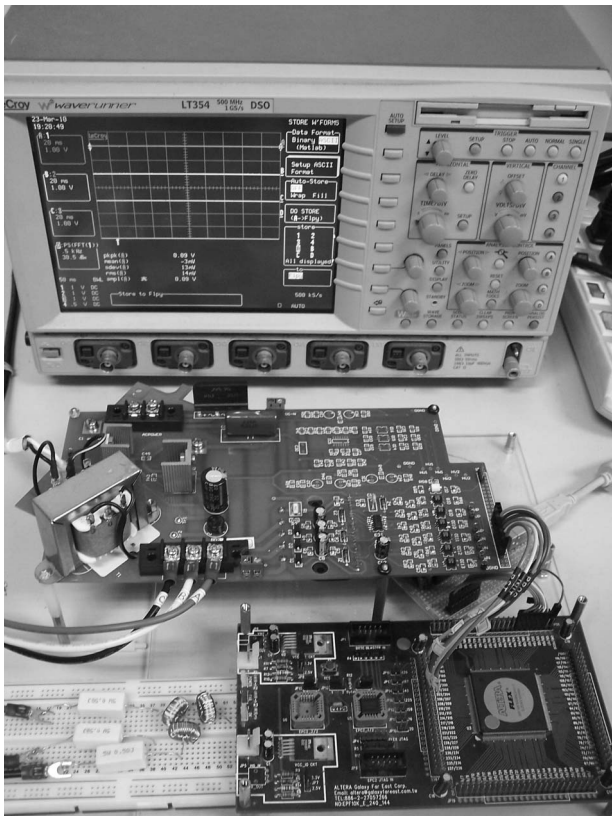

Fig. 8. Experimental platform.

IV. Design and Experimental Results

To compare the performances of MDFQM and SVPWM, both algorithms are implemented in the FPGA (FLEX10K100ARC). The block diagram of experimental platform is shown in Fig. 7. The three-phase sinusoidal comments sampled at 3 kHz are produced automatically by FPGA, and the outputs of FPGA are six control lines with 2.19-μs blocking time for each phase to prevent arm shooting through. The dc bus of the three-phase VSI is 10 V, and a y-connected RL load with a resistance of 8 Ω and an inductance of 0.33 mH is used. The experimental platform is shown in Fig. 8.

Two diagonal filter matrices $\mathbf{W}_1$ and $\mathbf{W}_2$ with diagonal terms $w_1 = z/(z-1)$ and $w_2 = z^2/(z^2-2z+1)$ are selected for comparison. $\mathbf{W}_1$ refers to MDFQM1, and $\mathbf{W}_2$ refers to MDFQM2. Fig. 9 shows the logic elements needed in FPGA to implement SVPWM, MDFQM1, and MDFQM2. Only one zero sequence, all phase legs connected to the ground, is used in SVPWM to have the minimum switching number and is denoted as DPWM [26]. The oversampling ratio of both

Total logic elements	3,246 / 4,992 (65 %)
Total pins	9 / 189 (4 %)
Total memory bits	0 / 49,152 (0 %)

(a)

Total logic elements	3,704 / 4,992 (74 %)
Total pins	9 / 189 (4 %)
Total memory bits	0 / 49,152 (0 %)

(b)

Total logic elements	1,284 / 4,992 (25 %)
Total pins	9 / 189 (4 %)
Total memory bits	0 / 49,152 (0 %)

(c)

Fig. 9. Logic elements needed to implement different modulators. (a) MDFQM1. (b) MDFQM2. (c) DPWM.

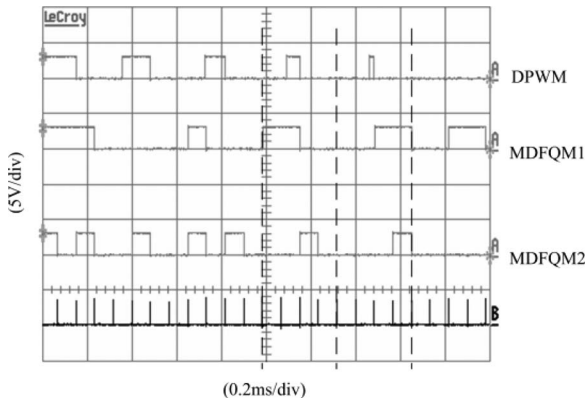

Fig. 10. Control signals for S_1 (see Fig. 1) produced by different modulators.

MDFQM1 and MDFQM2 is 4, such that the system is operated at 12 kHz and the minimum pulsewidth is 1/12 000 s. The bit resolution of DPWM is 8, such that the minimum pulsewidth is $1/(3k \times 2^8)$s. Since the carrier frequency of SVPWM is 3 kHz, the minimum switching number is $3k \times 4 = 12k$ per second. Fig. 10 shows the control signals for the upper switch of the first phase leg (S_1 in Fig. 1) produced by DPWM, MDFQM1, and MDFQM2. The frequency of the pulse signal (the fourth signal in Fig. 10) is 12 kHz, i.e., the time for which MDFQM1 and MDFQM2 update output controls. Once the output controls are updated according to the minimum error power, they will hold at the same states until the next pulse occurs. Different from MDFQM1 and MDFQM2, the control output of DPWM will switch twice within every four pulses, i.e., at a rate of 3 kHz.

A. Experimental Results for a Large Modulation Index

Three-phase sinusoidal waves with a frequency of 60 Hz and a modulation index of 0.5 are applied as reference signals. Notably, the maximum modulation index for DPWM is 0.577, without modification of the reference waveform (such as the third harmonic injection). Fig. 11 shows the time/frequency-domain analysis of the output current using the DPWM. Because of normal sampling, finite bit resolution, and dead-time effect, the frequency response of the DPWM has baseband harmonics. Figs. 12 and 13 show the analyses of MDFQM1

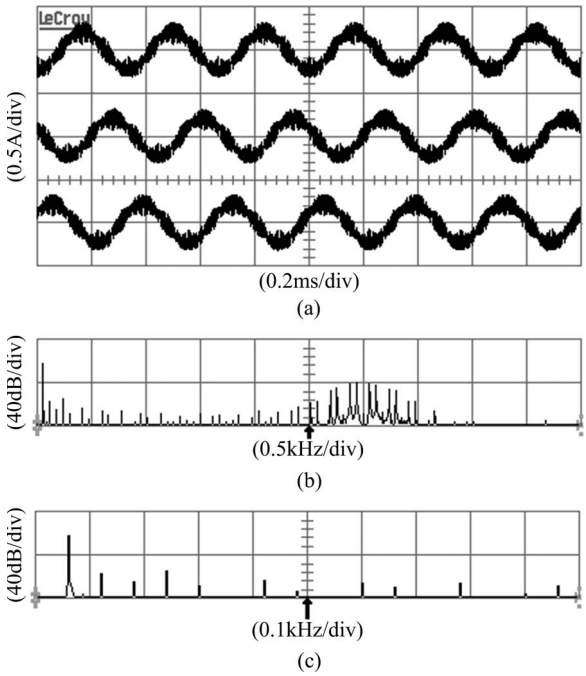

Fig. 11. Output current of VSI using DPWM. (a) Time-domain waveform of three-phase output currents. (b) Frequency-domain analysis of phase-a output current. (c) Zoom-in of (b) for low-frequency analysis.

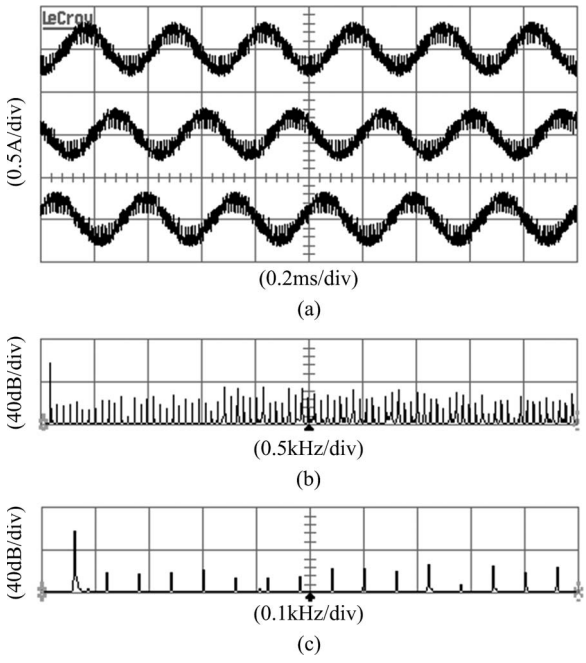

Fig. 12. Output current of VSI using MDFQM1. (a) Time-domain waveform of three-phase output currents. (b) Frequency-domain analysis of phase-a output current. (c) Zoom-in of (b) for low-frequency analysis.

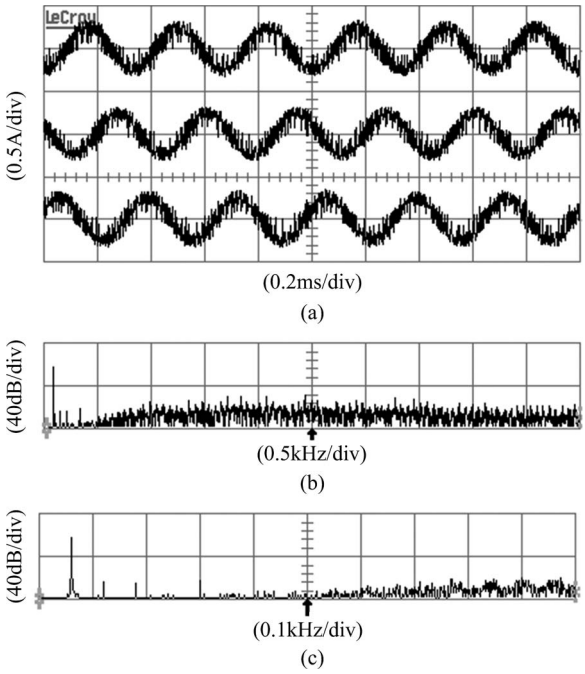

Fig. 13. Output current of VSI using MDFQM2. (a) Time-domain waveform of three-phase output currents. (b) Frequency-domain analysis of phase-a output current. (c) Zoom-in of (b) for low-frequency analysis.

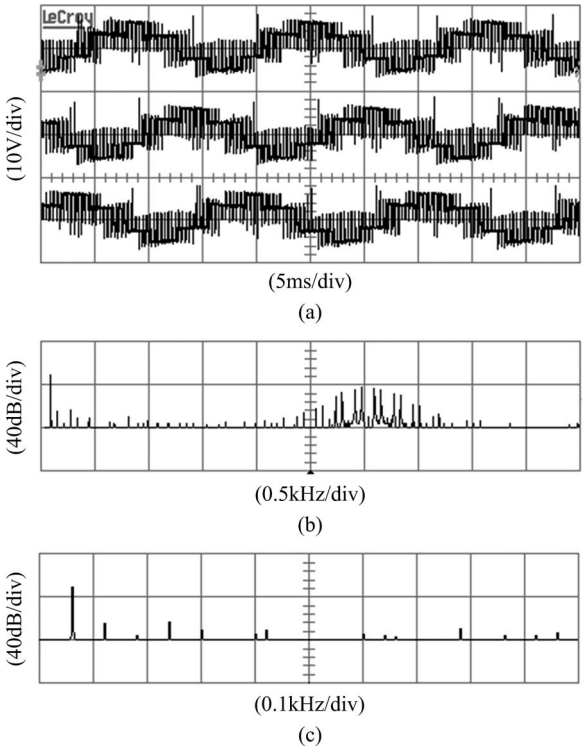

Fig. 14. Output phase voltage of VSI using DPWM. (a) Time-domain waveform. (b) Frequency-domain analysis of phase-a voltage. (c) Zoom-in of (b) for low-frequency analysis.

and MDFQM2, respectively. The frequency-domain analyses [Figs. 11–13(b)] show that SVPWM produces a narrow-band (tonal) noise while both MDFQM1 and MDFQM2 tend to spread the noise energy over a wider band. Therefore, the side-band noise (components around carrier frequency) is reduced using MDFQM1 and MDFQM2. For low-frequency analyses, Figs. 11–13(c) show the spectrum components within 1 kHz. MDFQM1 and MDFQM2 are likely to distribute the unwanted noise over the high-frequency band. As shown in Fig. 13(c), the noise components of MDFQM2 are relocated over 500 Hz, which separates noise components from the fundamental signal. The same results are found in the frequency analyses of phase voltages in Figs. 14–16.

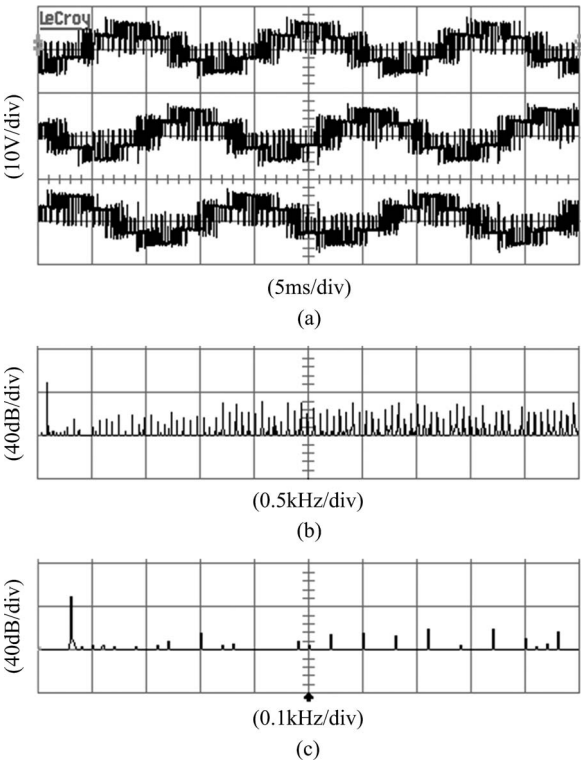

Fig. 15. Output phase voltage of VSI using MDFQM1. (a) Time-domain waveform. (b) Frequency-domain analysis of phase-a voltage. (c) Zoom-in of (b) for low-frequency analysis.

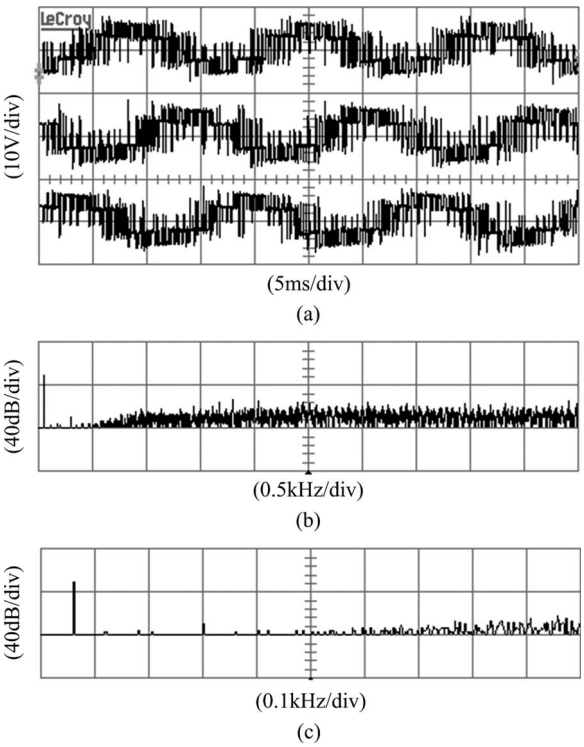

Fig. 16. Output phase voltage of VSI using MDFQM2. (a) Time-domain waveform. (b) Frequency-domain analysis of phase-a voltage. (c) Zoom-in of (b) for low-frequency analysis.

For a fair comparison, two cases are demonstrated: 1) the associated THD performance under a comparable switching number per unit time and 2) the associated switching number per unit time under a comparable performance of THD. To show the performance in terms of the number of switchings per unit time and THD, inputs with different frequencies are investigated. A single switching occurrence is defined as occurring when any one of the switches in the six-switch topology turns on and off once. Two different SVPWM strategies are used. CPWM refers to the centered SVPWM [15] which has the optimal THD performance [21]. The switching number of CPWM is six per input period. By choosing only one redundant state (zero state) [7], [9], [16], the switching number is reduced to four for each input period and is denoted as DPWM.

TABLE I
NUMBERS OF SWITCHINGS AND CURRENT THDS FOR CPWM, DPWM, MDFQM1, AND MDFQM2 AT DIFFERENT FREQUENCIES OF THE REFERENCE SIGNALS

Input Signal Frequency		40 Hz	60 Hz	80 Hz	100 Hz
No. of Switching per second ($\times 10^4$)	CPWM	1.8000	1.8000	1.8000	1.8000
	DPWM	1.1998	1.1878	1.1998	1.1398
	MDFQM1	1.1520	1.1160	1.1520	1.1400
	MDFQM2	1.0914	1.0966	1.1208	1.1056
Current THD within [0 3k] Hz (%)	CPWM	13.21	13.22	2.01	12.40
	DPWM	22.91	23.10	4.63	24.10
	MDFQM1	22.57	22.75	19.40	23.50
	MDFQM2	17.23	15.41	17.09	16.85
Current THD within [0 500] Hz (%)	CPWM	2.05	2.07	1.74	1.42
	DPWM	2.76	2.74	4.23	5.01
	MDFQM1	2.72	3.28	3.07	2.45
	MDFQM2	1.85	1.74	1.82	1.81

TABLE II
NUMBERS OF SWITCHINGS AND CURRENT THDS FOR CPWM, DPWM, AND MDFQM2 FOR A 60-HZ REFERENCE SIGNAL AT DIFFERENT MODULATION INDICES

Modulation index		0. 2	0.3	0.4	0.5
No. of Switching per second ($\times 10^4$)	CPWM	1.8000	1.8000	1.8000	1.8000
	DPWM	1.1878	1.1878	1.1878	1.1878
	MDFQM2	1.9731	1.7663	1.4502	1.0966
Current THD within [0 3k] Hz (%)	CPWM	8.05	9.42	11.16	13.22
	DPWM	54.33	44.33	32.98	23.10
	MDFQM2	22.21	16.05	17.58	15.41
Current THD within [0 500] Hz (%)	CPWM	3.58	3.13	2.28	2.07
	DPWM	2.50	2.55	2.86	2.74
	MDFQM2	2.53	1.66	1.52	1.74

Table I presents the switching number and the THD within 3 kHz and 500 Hz for different switching strategies, where current THD is calculated from phase currents. In this case, the switching numbers of both MDFQM1 and MDFQM2 are comparable with that of DPWM. The THD of MDFQM2 is lower than that of DPWM, while the THD of MDFQM1 is comparable with that of DPWM. Now, considering MDFQM2 and CPWM, the THD performances of both methods are about the same, but the switching number of MDFQM2 is about 2/3 of that of CPWM. Apparently, MDFQM2 can reduce the number of switchings without sacrificing the THD performance, indicating that the second-order feedback quantization system produces switching signals smartly and efficiently. Same

TABLE III
VOLTAGE THDS FOR CPWM, DPWM, MDFQM1, AND MDFQM2 AT DIFFERENT FREQUENCIES OF THE REFERENCE SIGNALS

Input Signal Frequency		40 Hz	60 Hz	80 Hz	100 Hz
Voltage THD within [0 3k] Hz (%)	CPWM	23.28	22.95	1.96	22.54
	DPWM	40.31	40.73	4.89	41.43
	MDFQM1	34.43	35.35	29.45	36.07
	MDFQM2	26.34	20.96	25.60	26.15
Voltage THD within [0 500] Hz (%)	CPWM	1.71	1.58	1.52	1.84
	DPWM	2.55	3.44	4.21	5.25
	MDFQM1	2.35	3.16	3.30	2.64
	MDFQM2	1.27	1.23	1.45	1.56

TABLE IV
VOLTAGE THDS FOR CPWM, DPWM, AND MDFQM2 FOR A 60-HZ REFERENCE SIGNAL AT DIFFERENT MODULATION INDICES

Modulation index		0. 2	0.3	0.4	0.5
Voltage THD within [0 3k] Hz (%)	CPWM	12.74	15.65	19.65	22.95
	DPWM	76.78	68.77	55.61	40.73
	MDFQM2	38.78	32.95	27.67	20.96
Voltage THD within [0 500] Hz (%)	CPWM	3.74	2.98	2.19	1.58
	DPWM	3.66	3.24	3.26	3.44
	MDFQM2	2.72	1.78	1.03	1.23

results are obtained when voltage signals are considered (see Table III). The method MDFQM2 outperforms DPWM/CPWM, suggesting that a higher order shaping filter is needed to enhance the performance of the proposed scheme.

B. Experimental Results for a Small Modulation Index

The experimental results, shown earlier, prove that the proposed method is useful when the modulation index is high. For a low-modulation index, Tables II and IV compare the performance of MDFQM2 with those of DPWM and CPWM for 60-Hz reference signals at various modulation indices. To maintain good THD performance, the switching number of MDFQM2 becomes higher than that of DPWM but still lower than that of CPWM within modulation indices $[0.3 \quad 0.5]$. The THD performances of MDFQM2 are comparable with that of CPWM within a frequency band of $[0 \quad 500]$ Hz, indicating a potential application of the proposed method in the control of the VSI.

V. CONCLUSION

MDFQM has been presented to produce control signals for a three-phase VSI. The method is formulated as a constrained optimization problem. System analysis demonstrates that SVPWM is a special case of MDFQM when the system is selected as a pure integrator.

The output voltages/currents of the MDFQM designs with different shaping filter matrices are compared to those of SVPWM in terms of both switching number and THD. The experimental results show that, at a large modulation index, the proposed technique can reduce the switching number (below that of CPWM) by almost 33% without increasing the THD. Second, with approximately the same switching number, the proposed MDFQM system produces a lower THD. At smaller modulation indices, the method can still maintain its performance within the input frequency band. Further studies of modulation index, stability of quantization methods for high-order shaping system, and n-phase systems are currently underway.

REFERENCES

[1] J. A. Houldsworth and D. A. Grant, "The use of harmonic distortion to increase the output voltage of a three-phase PWM inverter," *IEEE Trans. Ind. Appl.*, vol. IA-20, no. 5, pp. 1224–1228, Sep./Oct. 1984.

[2] K. Zhou and D. Wang, "Relationship between space-vector modulation and three-phase carrier-based PWM: A comprehensive analysis," *IEEE Trans. Ind. Electron.*, vol. 49, no. 1, pp. 186–196, Feb. 2002.

[3] O. Lopez, J. Alvarez, J. Doval-Gandoy, and F. D. Freijedo, "Multilevel multiphase space vector PWM algorithm with switching state redundancy," *IEEE Trans. Ind. Electron.*, vol. 56, no. 3, pp. 792–804, Mar. 2009.

[4] Y. H. Liu, C. L. Chen, and R. J. Tu, "A novel space-vector current regulation scheme for a field-oriented-controlled induction motor drive," *IEEE Trans. Ind. Electron.*, vol. 45, no. 5, pp. 730–737, Oct. 1998.

[5] D. W. Chung, J. S. Kim, and S. K. Sul, "Unified voltage modulation technique for real-time three-phase power conversion," *IEEE Trans. Ind. Appl.*, vol. 34, no. 2, pp. 374–380, Mar./Apr. 1998.

[6] D. G. Holmes, "The significance of zero space vector placement for carrier-based PWM schemes," *IEEE Trans. Ind. Appl.*, vol. 32, no. 5, pp. 1122–1129, Sep./Oct. 1996.

[7] A. Trzynadlowski and S. Legowski, "Minimum-loss vector PWM strategy for three-phase inverter," *IEEE Trans. Power Electron.*, vol. 9, no. 1, pp. 26–34, Jan. 1994.

[8] A. M. Hava, R. Kerkman, and T. A. Lipo, "Carrier-based PWM-VSI overmodulation strategies: Analysis, comparison, and design," *IEEE Trans. Power Electron.*, vol. 13, no. 4, pp. 674–689, Jul. 1998.

[9] A. Trzynadlowski, R. L. Kirlin, and S. Legowski, "Space vector PWM technique with minimum switching losses and variable pulse rate," *IEEE Trans. Ind. Electron.*, vol. 44, no. 2, pp. 173–181, Apr. 1997.

[10] S. R. Bowes and Y.-S. Lai, "The relationship between space-vector modulation and regular-sampled PWM," *IEEE Trans. Ind. Electron.*, vol. 44, no. 5, pp. 670–679, Oct. 1997.

[11] N. V. Nho and M. J. Youn, "Comprehensive study on space-vector-PWM and carrier-based-PWM correlation in multilevel inverters," *Proc. Inst. Elect. Eng.—Electr. Power Appl.*, vol. 153, no. 1, pp. 149–158, Jan. 2006.

[12] A. Iqbal and S. Moinuddin, "Comprehensive relationship between carrier-based PWM and space vector PWM in a five-phase VSI," *IEEE Trans. Power Electron.*, vol. 24, no. 10, pp. 2379–2390, Oct. 2009.

[13] Z. J. Shen, Y. Xiong, X. Cheng, Y. Fu, and P. Kumar, "Power MOSFET switching loss analysis: A new insight," in *Conf. Rec. 41st IEEE IAS Annu. Meeting*, Oct. 8–12, 2006, pp. 1438–1442.

[14] B. J. Arnet and J. P. Deyst, "Distribution of space-vector PWM conduction losses," U.S. Patent 0 044 472 A1, Apr. 18, 2002.

[15] B. P. McGrath, D. G. Holmes, and T. Meynard, "Reduced PWM harmonic distortion for multilevel inverters operating over a wide modulation range," *IEEE Trans. Power Electron.*, vol. 21, no. 4, pp. 941–949, Jul. 2006.

[16] Z. Yu, "Space-vector PWM with TMS320C24x/F24x using hardware and software determined switching patterns," Texas Instruments, Dallas, TX, Application Rep. SPRA524, Mar. 1999.

[17] A. R. Beig, G. Narayanan, and V. T. Ranganathan, "Modified SVPWM algorithm for three level VSI with synchronized and symmetrical waveforms," *IEEE Trans. Ind. Electron.*, vol. 54, no. 1, pp. 486–494, Feb. 2007.

[18] O. Lopez, J. Alvarez, J. Doval-Gandoy, and F. D. Freijedo, "Multilevel multiphase space vector PWM algorithm," *IEEE Trans. Ind. Electron.*, vol. 55, no. 5, pp. 1933–1942, May 2008.

[19] A. Das, K. Sivakumar, R. Ramchand, C. Patel, and K. Gopakumar, "A pulsewidth modulated control of induction motor drive using multilevel 12-sided polygonal voltage space vectors," *IEEE Trans. Ind. Electron.*, vol. 56, no. 7, pp. 2441–2449, Jul. 2009.

[20] A. Gopinath, A. S. Aneesh Mohamed, and M. R. Baiju, "Fractal based space vector PWM for multilevel inverters—A novel approach," *IEEE Trans. Ind. Electron.*, vol. 56, no. 4, pp. 1230–1237, Apr. 2009.

[21] B. P. McGrath, D. G. Holmes, and T. A. Lipo, "Optimized space vector switching sequences for multilevel inverters," *IEEE Trans. Power Electron.*, vol. 18, no. 6, pp. 1293–1301, Nov. 2003.

[22] G. Narayanan, D. Zhao, H. K. Krishnamurthy, R. Ayyanar, and V. T. Ranganathan, "Space vector based hybrid PWM techniques for

reduced current ripple," *IEEE Trans. Ind. Electron.*, vol. 55, no. 4, pp. 1614–1627, Apr. 2008.
[23] A. Mehrizi-Sani and S. Filizadeh, "An optimized space vector modulation sequence for improved harmonic performance," *IEEE Trans. Ind. Electron.*, vol. 56, no. 8, pp. 2894–2903, Aug. 2009.
[24] D. E. Quevedo and G. C. Goodwin, "Multi-step optimal analog-to-digital conversion," *IEEE Trans. Circuits Syst. I, Reg. Papers*, vol. 52, no. 3, pp. 503–515, Mar. 2005.
[25] J. S. Hu and K. Y. Chen, "A novel switch mode amplifier design for actuator array using MIMO optimal feedback quantization," in *Proc. Amer. Control Conf.*, New York, Jul. 11–13, 2007, pp. 2612–2617.
[26] L. Dalessandro, S. D. Round, U. Drofenik, and J. W. Kolar, "Discontinuous space-vector modulation for three-level PWM rectifiers," *IEEE Trans. Power Electron.*, vol. 23, no. 2, pp. 530–542, Mar. 2008.

Jwu-Sheng Hu (M'94) received the B.S. degree from the Department of Mechanical Engineering, National Taiwan University, Taipei, Taiwan, in 1984 and the M.S. and Ph.D. degrees from the Department of Mechanical Engineering, University of California, Berkeley, in 1988 and 1990, respectively.

From 1991 to 1993, he was an Assistant Professor with the Department of Mechanical Engineering, Wayne State University, Detroit, MI, where he received the Research Initiation Award from the National Science Foundation. Since 1993, he has been with the Department of Electrical Engineering, National Chiao Tung University, Hsinchu, Taiwan, where he became a full Professor in 1998 and has been the Vice-Chairman since 2006. Since 2008, he has been working part time at the Industrial Technology Research Institute, Hsinchu, where he serves as the Advisor for the Intelligent Robotics Program and the Principal Investigator of the Robotics Research Project funded by the Ministry of Economic Affairs. He also serves as a part-time Research Faculty with the National Chip Implementation Center (CIC), Taipei, for embedded system design applications. His current research interests include robotics, mechatronics, microphone array, and embedded systems.

Keng-Yuan Chen (S'07) received the B.S. degree from the Department of Electrical and Control Engineering, National Chiao Tung University, Hsinchu, Taiwan, in 2003 and the M.S. degree from the Department of Electrical and Control Engineering, National Chiao Tung University, in 2005, where she is currently working toward the Ph.D. degree.

Her main research interests include digital signal processing and class-D amplification.

Te-Yang Shen received the B.S. degree from the Department of Mechanical Engineering, Yuan Ze University, Jhongli, Taiwan, in 1997 and the M.S. degree from the Department of Mechanical Engineering, National Chung Cheng University, Chiayi, Taiwan, in 1999. He is currently working toward the Ph.D. degree in the Department of Electrical and Control Engineering, National Chiao Tung University, Hsinchu, Taiwan.

His main research interests include motor design and motor control.

Chi-Him Tang received the B.S. degree from the Department of Electrical and Control Engineering, National Chiao Tung University, Hsinchu, Taiwan, in 2008, where he is currently working toward the M.S. degree.

His main research interests include intelligent mobile robots, embedded systems, and brushless dc motor control.